

CHAPTER 44

REFLECTION FROM SWASH ZONE ON NATURAL BEACHES

Susumu Kubota¹, Masaru Mizuguchi² and Mitsuo Takezawa³

ABSTRACT

For separating incident and reflected waves, three methods based on linear long-wave theory, small-amplitude wave theory, and quasi-nonlinear long-wave theory were applied to field data recorded on a steeply sloping beach and on a gently sloping beach. The method based on the quasi-nonlinear long-wave theory gave the best results and described well the observed, incident, and reflected wave field.

I INTRODUCTION

The understanding of wave dynamics in the swash zone on natural beaches is important for determining beach erosion, designing coastal structures, and estimating beach deformation after the construction of such structures. However, the properties of the waves are not yet well understood because measurement of waves on natural beaches is difficult to perform. The authors measured the swash oscillation and waves and wave particle velocities in the surf zone by using 16 mm memo-motion cameras, capacitance-type wave gages, and electromagnetic current meters. A part of the results was presented at the 21st Coastal Engineering Conference (Takezawa et al., 1988), where separation of the incident and reflected waves was carried out with good results using the linear long-wave theory. However, application of the linear long-wave theory to field data collected later at a gentle beach gave poor results. Therefore, the small-amplitude wave and the quasi-nonlinear long wave theories were employed for the wave separation. The small-amplitude wave theory

1 Research Associate, Dept. of Civil Eng., College of Science and Technology, Nihon University, Kanda-Surugadai 1-8-14, Chiyoda-ku, Tokyo 101 Japan.

2 Dr. Eng., Professor, Dept. of Eng., Faculty of Science and Technology, Chuo University, Kasuga 1-13-27, Bunkyo-ku, Tokyo 112 Japan

3 Dr. Eng., Professor, Dept. of Civil Eng., College of Science and Technology, Nihon University

did not improve the previously obtained results. However, using the quasi-nonlinear long-wave theory produced better results. The present paper describes the analytical procedures and the results from analysis of the field observations.

11 THEORETICAL BACKGROUND FOR SEPARATING INCIDENT AND REFLECTED WAVES

2.1 Method Based on Linear Long-wave Theory

The separation method which employs linear long-wave theory was given by Guza, Thornton and Holman (1984),

$$\eta_I = \frac{1}{2} \left\{ \eta + \alpha \left[\frac{h}{g} \right]^{1/2} u \right\} \text{----- (1)}$$

$$\eta_R = \frac{1}{2} \left\{ \eta - \alpha \left[\frac{h}{g} \right]^{1/2} u \right\} \text{----- (2)}$$

where η , η_I and η_R are the water surface elevation of the observed, incident and reflected waves, u is the on-offshore component of water particle velocity, g is the acceleration due to gravity, h is the water depth, and α is a constant. The constant α theoretically takes the value of unity.

2.2 Method Based on Small-amplitude Wave Theory

If it is assumed that the observed wave is a result of linear superposition of the incident and reflected waves, then,

$$\eta = \eta_I + \eta_R \text{----- (3)}$$

$$u = u_I - u_R \text{----- (4)}$$

where u_I and u_R are the on-offshore component of water particle velocity of the incident and reflected waves respectively. It is also assumed that the incident wave is a sum of sinusoidal waves with different frequencies. Then, the following expressions are obtained,

$$\eta_I = \sum_{i=1}^{\infty} A_i \cos(\sigma_i t + \epsilon_i) \text{----- (5)}$$

$$\left. \begin{aligned} u_I &= \sum_{i=1}^{\infty} H_i A_i \cos(\sigma_i t + \epsilon_i) \\ H_i &= \frac{\sigma_i \cosh k_i (h+z)}{\sinh k_i h} \\ \sigma_i^2 &= g k_i \tanh k_i h \end{aligned} \right\} \text{----- (6)}$$

where t is the time, z is the vertical distance taking the origin of the coordinate system at the still sea water level, $\sigma_i = 2\pi / T_i$, $k_i = 2\pi / L_i$, and A_i , ε_i , L_i , and T_i are the wave amplitude, the phase difference, wavelength and wave period of an elementary wave. Expression for u_R is similarly,

$$u_R = \sum_{i=1}^{\infty} H_i B_i \cos(\sigma_i t + \varepsilon_i') \text{ ----- (7)}$$

where B_i and ε_i' are the amplitude and the phase difference. A finite Fourier series is used for expressing u as,

$$u = \sum_{i=1}^N (C_i \cos \sigma_i t + D_i \sin \sigma_i t) \text{ ----- (8)}$$

where C_i and D_i are the Fourier coefficients. A sum of independent elementary waves is considered, therefore, or each elementary wave, the following relation can be stated:

$$\begin{aligned} C_i \cos \sigma_i t + D_i \sin \sigma_i t \\ = H_i A_i \cos(\sigma_i t + \varepsilon_i) - H_i B_i \sin(\sigma_i t + \varepsilon_i') \text{ ----- (9)} \end{aligned}$$

Dividing both sides of Eq. 9 by H_i and adding terms i from 1 to N , we have:

$$\begin{aligned} \sum_{i=1}^N \frac{1}{H_i} (C_i \cos \sigma_i t + D_i \sin \sigma_i t) \\ = \sum_{i=1}^N A_i \cos(\sigma_i t + \varepsilon_i) - \sum_{i=1}^N B_i \sin(\sigma_i t + \varepsilon_i') = \eta_I - \eta_R \text{ ----- (10)} \end{aligned}$$

From Eq. (10) and Eq. (3), the final equations for the wave separation is obtained as:

$$\eta_I = \frac{1}{2} \left\{ \eta + \sum_{i=1}^N \frac{1}{H_i} (C_i \cos \sigma_i t + D_i \sin \sigma_i t) \right\} \text{ ----- (11)}$$

$$\eta_R = \frac{1}{2} \left\{ \eta - \sum_{i=1}^N \frac{1}{H_i} (C_i \cos \sigma_i t + D_i \sin \sigma_i t) \right\} \text{ ----- (12)}$$

A problem is the proper choice of N . Measurement noise is usually inherent in the high-frequency region. The power of the noise becomes predominant if a large number is taken on N . Thus, a suitable value on N must be chosen.

2.3 Method Based on Quasi-nonlinear Long-wave Theory

Ignoring any interaction between the incident and reflected wave, it may be assume that Eqs. (3) and (4) are valid. The basic equations in nonlinear long-wave theory of constant depth becomes:

$$\frac{\partial \eta}{\partial t} + \frac{\partial}{\partial x} \{ (h + \eta) u \} = 0 \quad \text{-----} \quad (13)$$

$$\frac{\partial u}{\partial t} + u \frac{\partial u}{\partial x} + g \frac{\partial \eta}{\partial x} = 0 \quad \text{-----} \quad (14)$$

Expanding u in a series and considering up to second order, the following relation between u and η is assumed:

$$u = \left[\frac{g}{h} \right]^{1/2} \eta + \beta \eta^2 \quad \text{-----} \quad (15)$$

Substituting Eq. (15) into the equation of continuity, Eq. (13), β is determined:

$$\beta = -\frac{1}{h} \left[\frac{g}{h} \right]^{1/2} \quad \text{-----} \quad (16)$$

Equation (16) does not satisfy the equation of motion, Eq. (14). In order to satisfy Eq. (14), β should be:

$$\beta = -\frac{1}{2h} \left[\frac{g}{h} \right]^{1/2} \quad \text{-----} \quad (17)$$

Equation (14) itself is originally only approximately correct for the real waves, and the second order terms of Eq. (14) partially vanish. Therefore, it was assumed that Eqs. (13) and (14) would be better satisfied if Eq. (16) was used instead of Eq. (17). Substituting Eq. (16) into Eq. (15):

$$u = \left[\frac{g}{h} \right]^{1/2} \eta \left(1 - \frac{\eta}{h} \right) \quad \text{-----} \quad (18)$$

From Eqs. (3), (4) and (18), Eqs. (19) and (20) result in

$$\eta_I = \frac{1}{2} \left\{ \eta + \alpha u \left[\frac{h}{g} \right]^{1/2} \frac{h}{h - \eta} \right\} \quad \text{-----} \quad (19)$$

$$\eta_R = \frac{1}{2} \left\{ \eta - \alpha u \left[\frac{h}{g} \right]^{1/2} \frac{h}{h - \eta} \right\} \quad \text{-----} \quad (20)$$

III FIELD OBSERVATIONS

3.1 Field Observation Sites

Data analyzed here were measured at Oarai Beach on July 29 (Takezawa et al., 1988) and at Hasaki Beach on July 30, 1987. Oarai Beach is located about 100 km north of Tokyo facing the Pacific Ocean. The Beach is bounded by a commercial harbor at its northern end, and groins were constructed for protecting the harbor against intruding sand from the south. Sand accumulates immediately south of groins and erosion is occurring in an area approximately 2 km south of the largest groin. The observation site was located approximately 1.8 km south of the largest groin. The sand in the swash zone was well sorted with a median diameter of 0.45 mm and a sorting coeffi-

cient, defined as $S=d_{75}/d_{25}$, where d_p is the grain diameter at which p percent of the sand weight is finer, of around 1.25.

Hasaki Beach is located at the southern part of Tokai Coast facing the Pacific Ocean about a distance of 100 km from Tokyo. A research pier belonging to the Hasaki Oceanographical Research Facility, the Port and Harbor Research Institute, Ministry of Transportation, is located here for facilitating field studies in the nearshore zone. The average tidal range at the beach is about 1.2 m and beach slope was considered to be gentle. The beach is composed of sand with a grain size in the range of 0.1 to 0.5 mm. The median grain diameter on the swash zone was around 0.18 mm. Figure 1 shows a location map of the field observation sites.

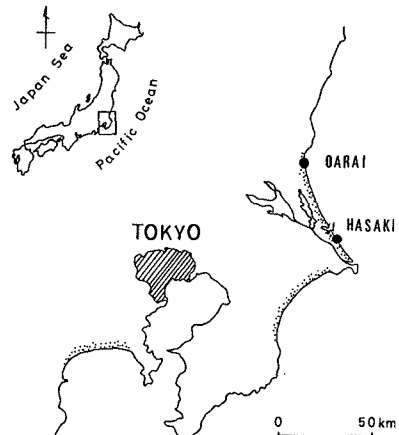


Fig. 1 Location map of field sites.

3.2 Measurement Procedure

Figure 2 shows the beach profile and the arrangement of the instrumentation at both beaches ((a) at Oarai Beach and (b) at Hasaki Beach).

In the swash zone, a target stick array of iron bars painted yellow was installed normal to the shoreline for photographic recording by 16 mm memo-motion cameras. The stick array consisted of 41 bars with an interval of 50 cm covering 20 m of the swash zone at Oarai and of 31 bars with an interval of 1 m covering 30 m of the swash zone at Hasaki. For photographing the waves from the side, a scaffold was elevated at the midpoint of the swash zone approximately 50 m south of the stick array at Oarai. Two sets of cameras recorded the waves from the scaffold. At Hasaki, waves in the swash zone were photographed by two sets of cameras on the pier.

The run-up meter, a capacitance-type wave gage with a modified measuring range, was also stretched parallel to the stick array and 50 cm beside it. The capacitance wire was held at a constant height of 2 cm above the sand surface by supporting rods installed at an interval of 2 m. A plastic scale was pasted to each supporting rods. In order to keep the wire at a constant height, two men were engaged in adjusting the movable supporting device of the wire to follow the sand surface fluctuations.

To record the sea surface variation, target poles for the 16 mm cameras were installed in the sea. A capaci-

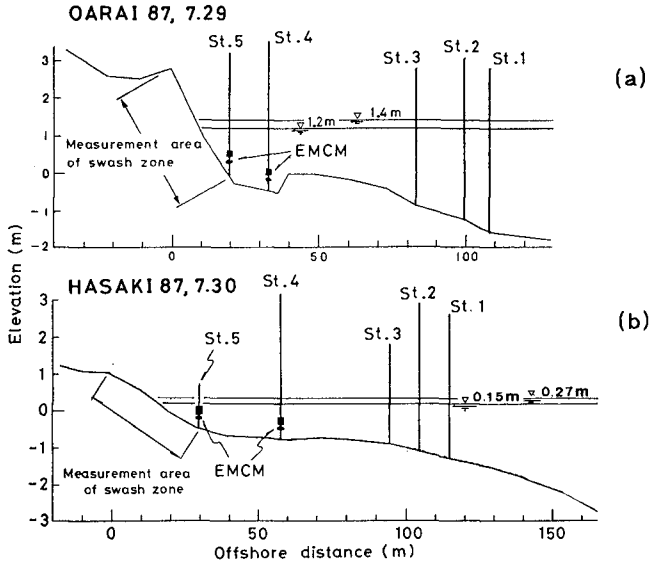


Fig. 2 Beach profiles and arrangement of measuring instruments.

tance-type wave gage and a two-component electromagnetic current meter (EMCM) were attached to the target poles of St. 4 and St. 5 at both beaches. Waves were photographed by two sets of 16 mm cameras on a scaffold elevated at the berm crest at Oarai and on the pier at Hasaki. Figure 3 shows the arrangement of the sticks on the swash slope.

At Oarai, data collection was started on 16:10 and ended 17:50, giving a 100 min experimental duration. During the experiment the tide rose about 20 cm. Average breaking wave height and period estimated by visual observation were about 1m and 12 sec. The average breaker line was located between Sts. 2 and 3. The type of breaker was plunging and the wave direction was almost normal to the shoreline. Additional information may be found in Takezawa et al. (1988). At Hasaki the measurements started on 17:15 and ended on 18:31, with seventy six minutes of data collection. During the measurements the tide rose about 20 cm. The average breaker line was located near St. 2 and an

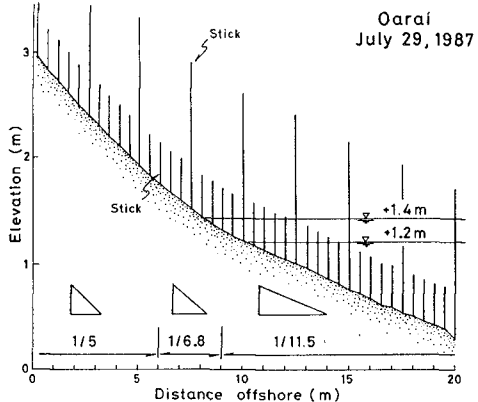


Fig. 3 (a)

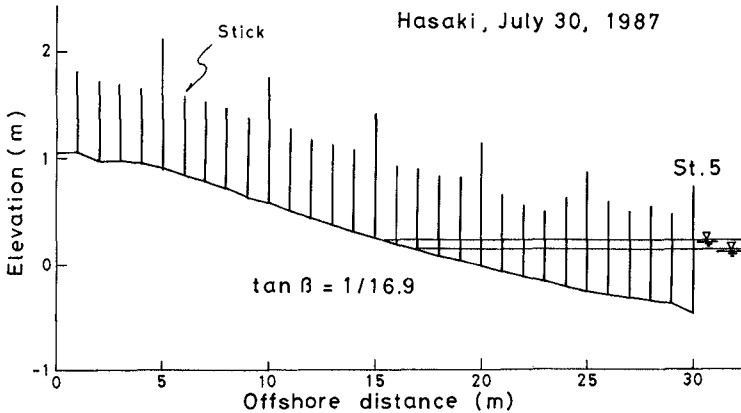


Fig. 3(b) arrangement of the sticks on the swash slope.

average breaking wave height of 0.95 m and a wave period of 12.1 sec were recorded. The waves broke as the plunging type.

Analyzing data obtained by EMC, no significant power was found in the longshore velocity at both sites except in the very low frequency range.

IV WAVE SEPARATION

In the following, results analyzed at St.4 on Oarai Beach (Hereafter this case will be abbreviated as OA87.St.4) and St.4 on Hasaki Beach (Hereafter abbreviated as HA87.St.4) are described and discussed. Wave data obtained by 16 mm cameras were analyzed in the present study and the wave data obtained with the capacitance-type wave gages were not employed.

Before the results of the analysis are shown, some supplementary information is given. The data collection with the electrical instruments and the photographing with the 16 mm cameras were simultaneously started by hand. No electrical synchronization between the measuring systems were done. The target poles and the electromagnetic current meters were placed close to each other but they were not placed exactly at the same location. It is expected that there was some time lag between the sea surface variation and the water particle velocity. In order to find the time lag, cross-spectral analysis was carried out and the time lag of 0.6 sec (OA87.St.4) and 0.4 sec (HA87.St.4) were obtained between the data records. The time lag was removed in the later analysis.

In the wave separation using Eqs. (11) and (12), a suitable value of N had to be chosen. There are no guide lines for selecting a value of N . Therefore, considering the power spectral functions, three critical frequencies, 0.35 Hz, 0.6 Hz, and 1.0 Hz for OA87.St.4 and 0.4 Hz, 0.9 Hz and 1.2 Hz for HA87.St.4, were evaluated. The three chosen frequencies did not give any noticeable difference

when analyzing the data records. The results obtained for the frequency 1.0 Hz at OA87.St.4 and for 1.2 Hz at HA87.St.4 are discussed later.

In the wave separation using Eqs. (1) and (2) and Eqs. (19) and (20) a value of α has to be determined. The value of α was chosen as the ratio of $(\overline{\eta^2}/\overline{u^2})^{1/2}$ between the observed and the calculated from small-amplitude wave theory, in the primary frequency range of progressive wave domain.

The most suitable value α of was 1.54 for OA87.St.4 and 1.26 for HA87.St.4.

4.1 Wave Separation

Figure 4 shows a portion of the resolved waves by the three methods at OA87.St.4, and Fig. 5 displays results from HA87.St.4. The incident and corresponding reflected waves are easily identified for primary individual

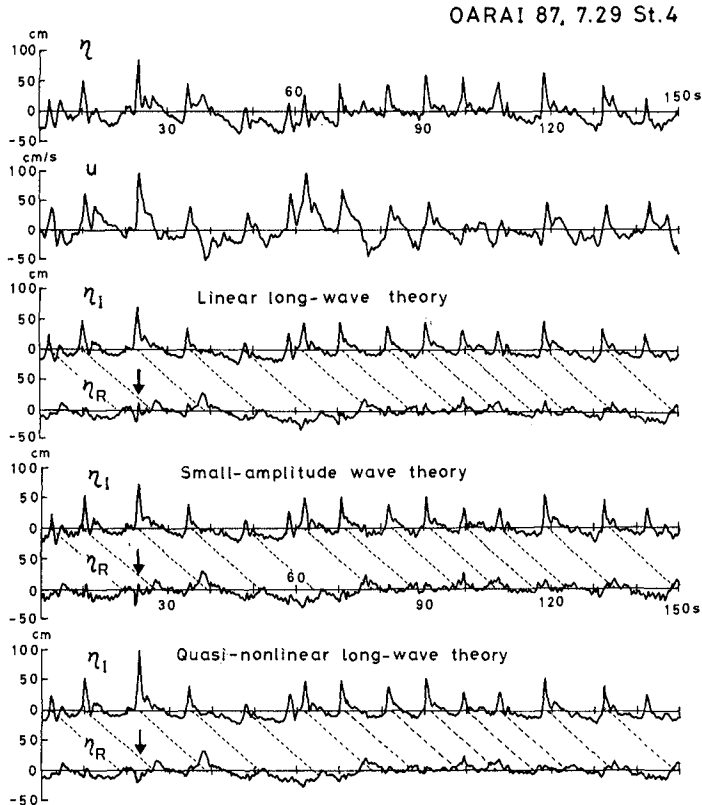


Fig. 4 Observed wave profiles, and separated incident and reflected wave profile by the three methods.

waves (Mizuguchi, 1982) at Oarai Beach, which had a steep swash zone slope. In contrast, reflected waves do not appear at Hasaki Beach, which had a gentle swash zone slope. It is difficult to recognize the correlation between the incident waves and the reflected waves, instead long-period waves appears predominantly in the reflected waves. This implies that primary individual waves ranging from about 5-20 sec in period, having the main power of the incoming waves, lost their energy in the swash zone, resulting in negligible reflection, and only the remaining long-period waves were reflected.

There is no standard method for determining the best separation technique. However, there is a tendency that an excess rise in sea water level appears for a portion of the reflected wave profile separated with linear long-wave theory (Eqs. (1) and (2)), and small-amplitude wave theory (Eqs. (11) and (12)), where this portion corresponds to the crest of the incident wave, when the reflected wave profiles are examined in detail.

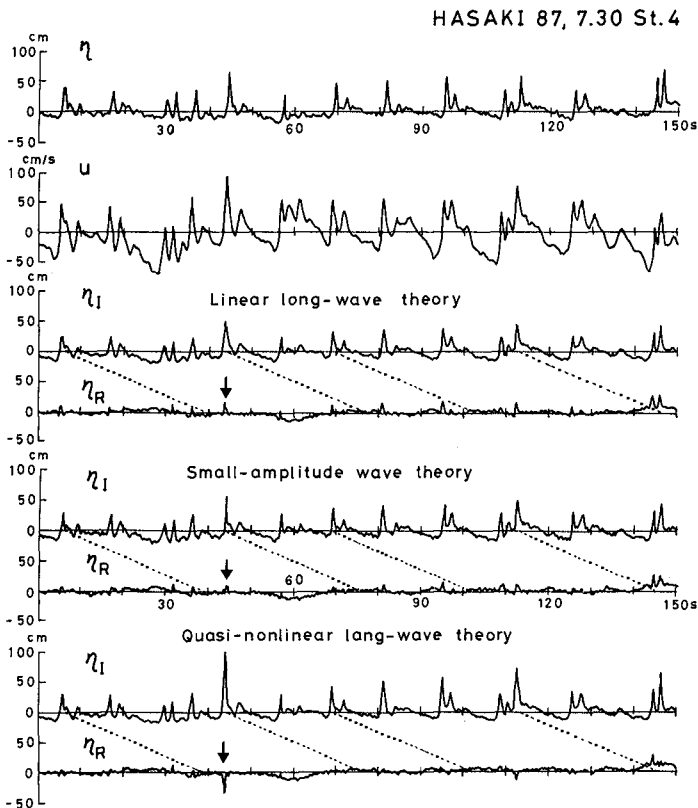


Fig. 5 Observed wave profiles, and separated incident and reflected wave profile by the three methods.

The excess rise does not appear in the reflected wave profile separated with the method based on quasi-nonlinear long-wave theory, (Eqs. (19) and (20)). An example is found at an elapsed time of 23 sec for OA87.St.4, indicated by arrows. This is because the water particle velocity is smaller to apply Eqs. (1) and (2), and Eqs. (11) and (12). However, in the reflected wave profiles separated using Eqs. (19) and (20) for HA87.St.4, an abrupt sharp depression is found at an elapsed time of 45 sec. This was due to an exceptionally large observed water particle velocity, although it is not clear why this occurred.

As a measure to evaluate the different methods, the cross-correlation functions between incident and reflected waves were calculated and are shown in Fig. 6. Close to the time lag zero, the cross-correlation function derived from small-amplitude wave theory and linear long-wave theory fluctuate in comparison with quasi-nonlinear long-wave theory for both OA87.St.4 and HA87.St.4. This means that wave separation using Eqs. (1) and (2) and Eqs. (11) and (12) involves some uncertainty. In addition, the value of the maximum cross-correlation coefficient obtained by the method based on Eqs. (19) and (20) was the highest among the three methods compared at OA87.St.4, where waves were highly reflected because of the steep swash slope. According to the preceding discussion, it is concluded that the separation method based on the quasi-nonlinear long-wave theory is the best among the three investigated methods.

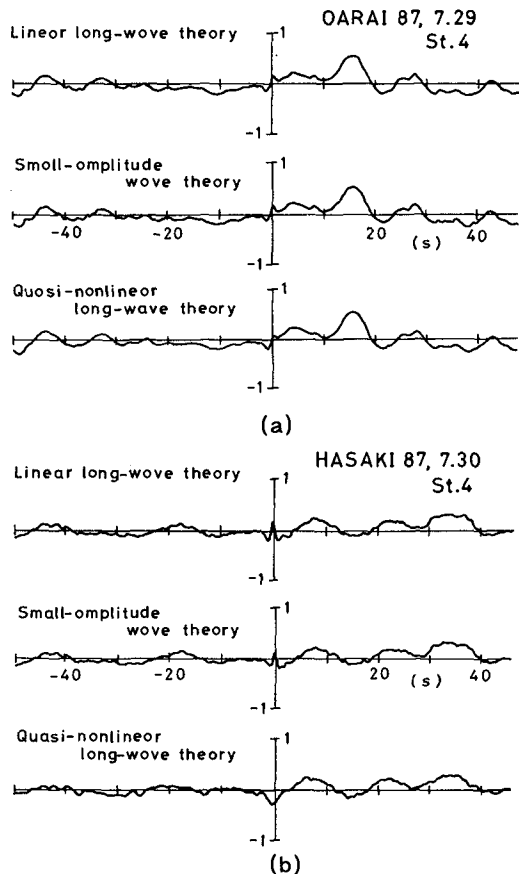


Fig. 6 Cross-correlation function between the incident and the reflected waves.

4.2 Spectral Considerations

Figure 7 shows the power spectral density function for the observed waves, and for incident and reflected waves at OA87. St.4 and HA87. St.4. Figure 8 shows the cross-spectral function between the incident and reflected waves.

At OA87. St.4, in the range below 0.15 Hz, which include the peak frequency, the power spectral shape of the incident and reflected waves are similar and the coherence function is nearly 1.0. This suggests that signifi-

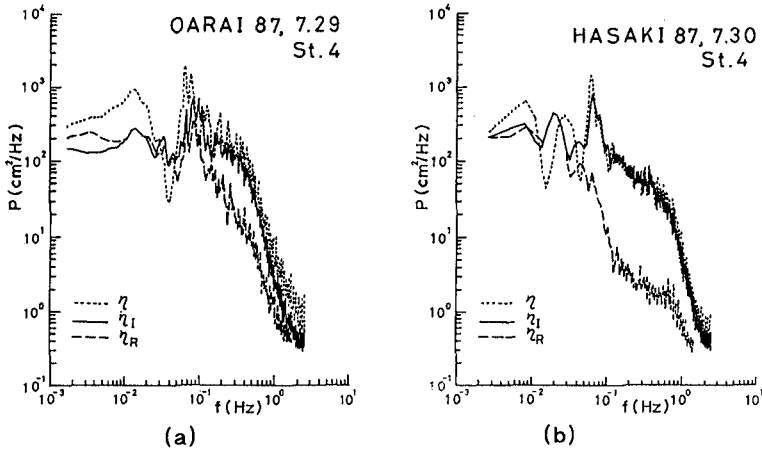


Fig. 7 The power spectral density function of the observed, incident and reflected waves.

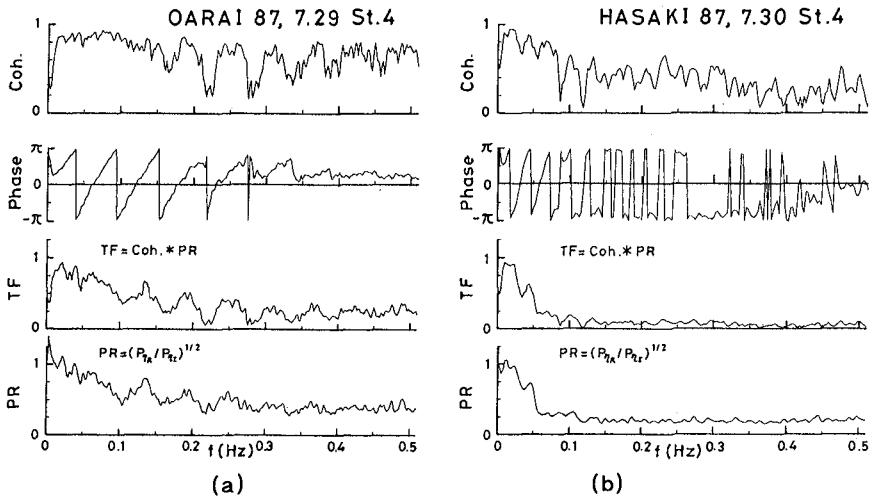


Fig. 8 Cross-spectral function between the incident and reflected waves.

cant wave reflection occurred. In the range higher than 0.15 Hz, the power of the reflected waves is considerably smaller than that of the incident waves. The energy in this range, were lost during the swash process, resulting in a small amount of reflection.

At HA87.St.4, in the range higher than 0.05 Hz, which includes the main power of the incident waves, the power of the reflected waves is very small compared with the power of incident waves, and coherence function is also small. In the range below 0.02 Hz, the power of the incident and reflected waves are of almost the same magnitude and coherence function is almost unity. This indicates that the significant reflection occurred only for long period components.

4.3 Joint Distribution of Wave Height and Period

Figure 9 shows the joint distribution of wave height and period for observed, incident, and reflected waves. The distribution of the observed waves is similar to that of the separated incident waves at both observation sites, OA87.St.4 and HA87.St.4, apart from that the distribution of the incident waves has two maxima. This implies two wave groups, with primary individual waves coming from the off-shore and secondary waves with small heights and periods mainly produced by disturbances in the surf zone. It was noted in the analysis of the

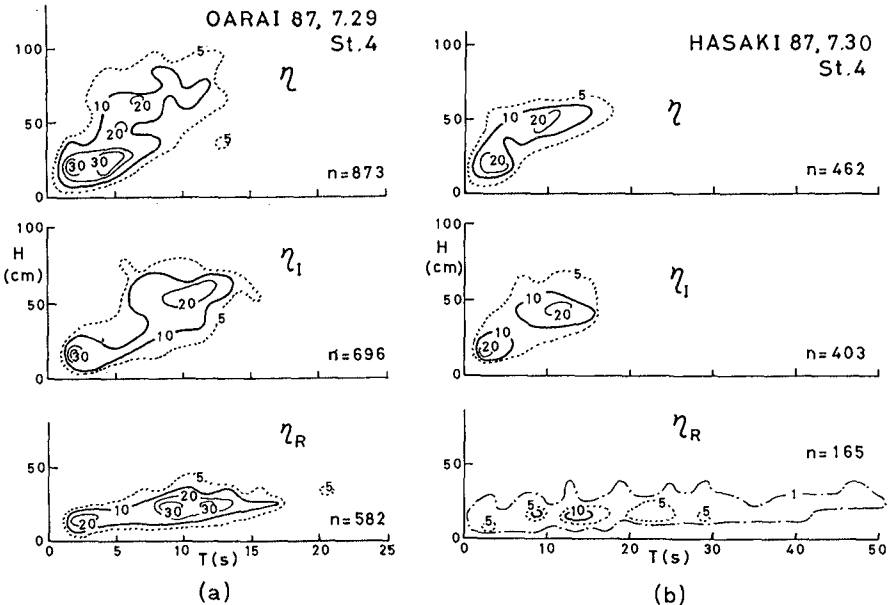


Fig. 9 The joint distribution of wave height and period for the observed, incident and reflected waves.

distributions of incident and reflected waves at OA87.St.4, that the number of defined waves somewhat decreased in the reflected wave field compared to the incident wave field, and the distribution of the reflected waves spread a little towards longer periods. However, the decrease in the number of waves mainly occurred for waves with small height and period, and the decrease did not occur for the primary individual waves ranging from 5 to 20 sec in period although they were reduced in height. This means that primary individual waves in the incident wave field return to the offshore with a decreased height.

The corresponding development does not appear for the waves at HA87.St.4. The number of defined waves considerably decreases and long-period waves not identified in the incident wave field appear in the reflected wave field. These long-period waves are found in the reflected wave profile in Fig. 4(b) and in the range below 0.06 Hz in the power spectral density function shown in Fig. 7(b). Thus, the waves that had the main energy in the period range 8 to 20 sec in the incident wave field lost their energy due to wave breaking on the slope and disappeared in the reflected wave field, implying no reflection. Instead, the long-period waves, which are difficult to distinguish in the incident wave field, are more easily identified in the reflected wave field. Following the above discussion, it is noted that the distribution of the observed waves at OA87.St4 is a result of superimposed incident and reflected waves, which does not show the proper characteristics of an incident wave distribution. The distribution of the observed waves at HA87.St.4 gives almost the same distribution as that of the incident waves. In summary, we need to consider wave reflection when the characteristics of incident waves on steep beaches are estimated.

V CONCLUDING REMARKS

The wave separation method based on quasi-nonlinear long-wave theory gave reasonable results using field data observed at a steeply sloping beach and also from a gently sloping beach. The separated incident and reflected wave field well described the wave characteristics in the surf zone, that is, high frequency waves lost their energy due to breaking and disappeared in the reflected wave field. The waves ranging in period from 5 to 20 sec, which have the main power of the incident waves and are ordinary wind waves, partially lost their energy due to wave breaking and returned to the offshore as reflected waves on the steep foreshore beach. Individual reflected waves were well related to the corresponding incident waves. However, on the gently sloping beach the waves lost their energy on the foreshore slope

and no reflection occurred. Low-frequency waves not easily identified in the incident wave field emerged in the reflected wave field and formed on-offshore standing waves without any breaking on the slope.

The critical frequencies to distinguish between perfect and partial reflection, and partial and no reflection depended on the gradient of the foreshore beach slope. Further field studies at beaches with different slopes should be carried out in order to qualify the wave characteristic in the nearshore zone. Also, further improvement of measurement instruments and development of the theoretical considerations are needed.

ACKNOWLEDGEMENTS

The authors would like to thank the Port and Harbor Research Institute, Ministry of Transportation, for permission to use the observation pier. We also gratefully acknowledge the assistance of Dr. S. Hotta, Professor, Dept. of Civil Eng., College of Science and Technology, Nihon University, during the field observation and in the preparation of this paper. We would also like to express our appreciation to our universities students who provided considerable supports during the field work. Without their help we could not have carried out this field experiment.

A portion of this study was supported by the Research Grant for Assistants and Young Researchers, Nihon University Research Grants for 1989 (Kubota) and Joint Research Grant, College of Science and Technology Research Grants for 1989, Nihon University (Takezawa and Kubota).

REFERENCES

- Guza, R. T., E. B. Thornton and R. A. Holman (1984): Swash on steep and shallow beaches, Proc. 19th Coastal Eng. Conf., ASCE, pp. 708-723.
- Mizuguchi, M. (1982): Individual wave analysis of irregular wave deformation in the nearshore zone, Proc. 18th Coastal Eng. Conf., ASCE, pp. 485-502.
- Takezawa, M., M. Mizuguchi, S. Hotta and S. Kubota (1988): Wave run-up on a natural beach, Proc. 21st Coastal Eng. Conf., ASCE, pp. 151-165.